Methodology for failure mode prediction of onshore buried steel pipelines subjected to reverse fault rupture

Vasileios E. Melissianos[1], Dimitrios Vamvatsikos[1] and Charis J. Gantes[1]

[1]Institute of Steel Structures, School of Civil Engineering, National Technical University of Athens

Corresponding Author: Vasileios E. Melissianos, Institute of Steel Structures, School of Civil Engineering, National Technical University of Athens, 9, Iroon Polytechneiou str., Zografou Campus, GR-15780, Athens, Greece, email: melissia@mail.ntua.gr

ABSTRACT: Oil and gas buried steel pipelines are vulnerable to permanent ground displacements, such as those resulting from tectonic fault activation. The dominant failure mechanism is strongly dependent on the type of faulting. The more complex case is the reverse fault type because the crossing pipeline is significantly compressed and bent and consequently, it may fail due to local buckling, upheaval buckling or tensile weld fracture. Which among those failure modes will be critical, depends on a set of parameters, comprising fault crossing geometry, diameter to thickness ratio (D/t) of the pipeline, pipeline steel grade, and backfill soil properties. An extensive parametric study is carried out, followed by statistical processing of the results in order to formulate simplified statistical models for the prediction of the predominant failure mode according to criteria set by the American Lifelines Alliance and EN 1998-4 standards. The study thus offers the first comprehensive attempt to quantify the qualitative criterion that deeply buried pipes with high D/t ratio tend to buckle locally, while shallowly buried pipes with a low D/t ratio tend to buckle globally. Pipe designers may use the provided expressions to predict the predominant failure mode in order to either apply the necessary seismic countermeasures or re-design the pipeline if necessary.

KEYWORDS: buried pipeline, reverse fault rupture, numerical model, failure modes, statistical analysis, simplified expressions

1. Introduction

Buried steel fuel pipelines are vital infrastructure of national and international importance that is vulnerable to earthquake-induced Permanent Ground Displacements (PGDs), such as those resulting from fault offset. In case of fault activation, the crossing pipeline’s integrity is severely threatened [1] with significant downtime, monetary losses, and even casualties. The mechanical behavior of a pipe subjected to faulting is primarily dictated by the fault type, contrary to the case of imposed transient ground displacements, such as those caused by ground shaking ([2]-[3]), where potential pipe failure depends on soil homogeneity. In case of strike-slip and normal faults, the pipeline is mainly tensioned and bent and the predominant failure mode is either local buckling of the pipeline wall or tensile fracture at the locations of welds between adjacent pipeline parts. Contrarily, in case of reverse faulting, the pipe is bent and mainly compressed, thus developing high compressive stresses may result to local and/or global instability. The principal parameters affecting pipe stability are the diameter to thickness (D/t) ratio that determines the cross-section slenderness and the burial depth that determines the soil pressure acting on the pipe. Soil resistance (i.e. stiffness and strength) to pipe upward movement in the trench is much lower than the resistance to pipe downward movement, which may contribute to the so-called upheaval buckling (beam-typ buckling), in which the compressed pipeline buckles globally and deforms upwards, often being exposed above the ground surface. Yun and Kyriakides have formulated in [4] a qualitative criterion stating that deeply buried pipes with high D/t ratio tend to buckle locally, while shallowly buried pipes with low D/t ratio tend to buckle globally.

The problem of the pipeline under faulting is displacement- and strain-controlled, as the imposed actions are in the form of soil displacement that the pipeline has to follow, while the pipeline response is often in the inelastic range. Hence, pipeline verification is carried out in strain, rather than in stress terms, exploiting steel ductility, as in EN 1998-4 [5], ALA [6] and CSA Z662 [7]. In these codes, limiting expressions are provided for tensile strains to avoid tensile fracture and for compressive strains to avoid local buckling of the pipe wall.

In recent years, an intensive effort is underway worldwide for the reliable assessment of pipe behavior under faulting through experimental, analytical and numerical studies. Analytical tools are very useful for the preliminary calculation of pipe maximum strain (indicatively [8]-[12]). Numerical modeling, employing the finite element method is adopted to account for material nonlinearity, pipe – soil interaction, pipe cross-section ovalization and local buckling in a more rigorous way. The beam-type model, considering the pipe as a beam resting on a nonlinear Winkler foundation, is the simpler numerical approach (indicatively [13]-[17]). The continuum 3D model, using shell elements for the pipe and solid elements for the soil, with contact elements at their interface, is employed to better assess pipe local buckling and cross-section ovalization (indicatively [18]-[22]). However, this model is significantly time-consuming and its application in engineering practice is cumbersome. Finally, experimental studies of pipes under PGDs in centrifuge or split-box tests (indicatively [23]-[27]) offer a deeper understanding of the pipe mechanical behavior but performing an experiment is constrained by high cost and geometrical restrictions.

In particular, the response of buried pipes under strike-slip and normal fault rupture has been thoroughly investigated during the last decades, starting from the pioneering work of Newmark and Hall [28]. Contrarily, the mechanical behavior of pipes under reverse fault rupture (Figure 1) has drawn the attention of researchers only recently.

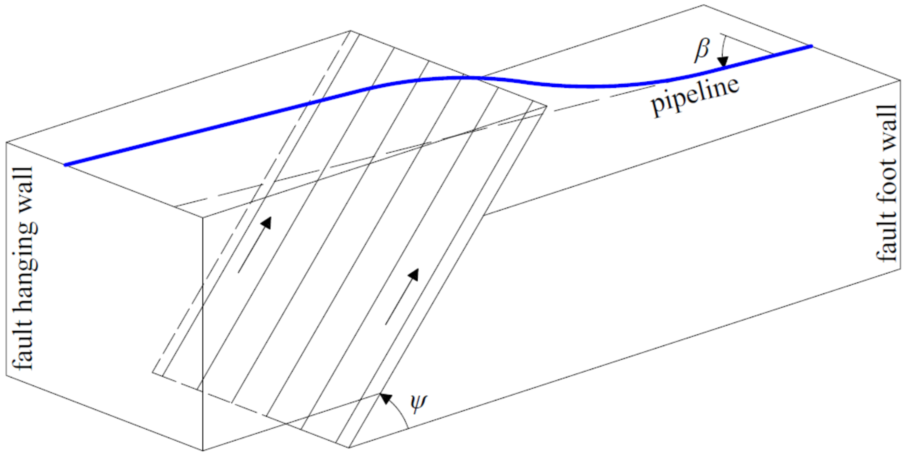

Figure 1: Pipeline – reverse fault crossing (fault dip angle: ψ, pipeline – fault crossing angle: β)

A detailed description of the beam-type FE model for pipes under reverse faulting has been firstly presented by Joshi et al. [14]. The authors concluded that compressive strains can be reduced by orienting the pipe to be near parallel to the fault trace and by trench backfilling with loose soil. Also, it was shown that the reduction of D/t ratio leads to the decline of compressive strains, increase of burial depth leads to the development of higher strains and, for a given fault dip angle, low crossing angle leads to pipe local buckling, while higher dip angle leads to pipe upheaval buckling.

Rojhani et al. [29] were the first to perform centrifuge tests of pipes subjected to reverse faulting. It was found that low burial depth and low D/t ratio lead to pipe upheaval buckling. Prevention of upheaval buckling can be achieved by increasing burial depth and pipe diameter. Rofooei et al. [30] carried out a parametric study of HDPE and steel pipes subjected to oblique-reverse faulting using the beam-type finite element model. It was mainly concluded that crossing angle is a key parameter for the level of compressive strains, HDPE pipes exhibit more compression that steel pipes, for constant pipe diameter the compressive strains increase with increasing D/t ratio, and pipes with low D/t ratio are more favorable in fault crossings.

Zhang et al. [31] employed the continuum FE model and found that the decrease of the D/t ratio leads to the reduction of the number locations that local buckling occurs, a decreased probability of pipe local buckling and the reduction of tensile and compressive strains. Jalali et al. [32] presented a series of experiments using a split-box to investigate the behavior of steel pipes under reverse faulting. Then, continuum numerical models were calibrated based on the experimental results. The authors found that the pipe rupture is more likely to occur in the hanging wall part and pipes in the tests exhibited “diamond-shaped” buckling. They, also, investigated the accuracy of ALA [6] expressions for soil-pipe interaction forces were investigated revealing that these expressions can be used for engineering purposes with acceptable accuracy. Liu et al. [33] employed a hybrid numerical model to examine the effect of steel properties on the development of local buckling in buried pipes under reverse fault movement. It was found that for a pressurized pipe the properties of steel affect the critical stress and fault displacement for local buckling occurrence, while steel yield stress and hardening parameter do not affect critical buckling strain. Liu et al. [34] examined the buckling failure modes of a high strength X80 steel gas pipeline and highlighted the nonlinearity of the problem employing the beam-type finite element model. The authors examined the effect of fault dip angle and wall thickness. The important observation was that if upheaval buckling is preceded then local buckling occurs shortly after for increasing reverse fault offset.

Xu and Lin [35] examined the effect of fault crossing geometry using a hybrid numerical model of a typical large diameter pipe with a high D/t ratio, being relatively deeply buried. It was found that for low angle ψ and near parallel pipe-fault orientation, the failure mode sequence was ovalization, local buckling, and tensile fracture. Moreover, for low angle ψ, the increase of angle β drives the local buckling location closer to the fault and for a pipe – fault perpendicular crossing ($\beta = 90^{\circ}$) the increase of dip angle ψ results to more pipe bending than compression, while the decrease of angle ψ leads to pipe failure for lower fault offset magnitude. Wijewickreme et al. [36] carried out full-scale experiments in a soil chamber modeling reverse faulting to investigate the mobilization of soil restraints on buried pipes and suggested to take into account the soil stiffness effects in a continuous basis in the analysis in order to achieve more reliable results. Jalali et al. [37] were the first to present results from shear-box experiments focusing on the soil rupture pattern, the magnitude of pipe strains and the cross-section distortion with reference to burial depth and relatively low D/t ratio.

Rofooei et al. [38] used shear-box experimental results in combination with numerical results to formulate new expressions for the uplift force on the basis of hose proposed by ALA [6] and PRCI [39]. Uplift soil force was found to be lower at sections close to the fault plane (distance up to $10D$) and higher at sections away from the fault.

Demirci et al. [40] presented a series of thorough 1g-scale experiments of pipes using a shear-box and corresponding numerical analysis, which concluded that bending strain increases with the increase of burial depth, larger bending strains usually develop on the pipe at the foot-wall and double curvature appears within the fault crossing zone, leading to pipe yielding. Cheng et al. [41] employed a continuum numerical model to investigate the effect of the underlying rock stratum in the failure analysis of a buried X80 pipeline under oblique-reverse fault rupture. The authors found that the three-dimensional fault movement affects the failure mode sequence and identified the corresponding effects of fault dip angle, internal pressure and D/t ratio, considering also the cross-section ovalization. Then, Tsatsis et al. [42] presented numerical and experimental results for buried pipes embedded in sandy soil focusing on the modeling of fault rupture propagation and axial soil resistance. It was found that the fault dip angle dominates pipe response and that pipe pressurization is detrimental. Finally, Zhang et al. [43] employed the continuum finite element model and examined the effect of internal pressure on the buckling behavior of pipes under faulting, concluding that high-pressure pipes are more prone to local buckling failure in case of reverse than strike-slip faulting.

Published results have improved the understanding of pipe behavior and have revealed the basic aspects of the failure mode sequence. However, the qualitative criterion of Yun and Kyriakides [4] that shallowly buried pipes with low D/t ratio tend to buckle globally, while deeply buried pipes with high D/t ratio tend to buckle locally, has not been quantitatively addressed in depth until now, due to the multi-parametric nature of the problem. Research on upheaval buckling is mainly focused on unburied or partially buried submarine pipelines. In this case, thermal expansion is the primary cause of pipeline lateral or upheaval buckling on the seabed, as indicatively presented in [44]-[46]. Contrariwise, research on upheaval buckling of onshore pipes subjected to significant compression due to reverse faulting is limited. It is worth noting that the upheaval buckling of onshore pipes under reverse faulting is not directly addressed in codes. A general qualitative provision for pipeline design against upheaval buckling is given only in CSA Z662 [7]. This type of buckling may not lead directly to a loss of content, but the pipe's serviceability is impacted due to the significant structural deformation. Moreover, it has been found that upheaval buckling may be followed by local buckling for a relatively low increase of fault offset [34], [35]. Thus, the upheaval buckling of buried pipelines is treated as a failure mode.

The scope of this study is to provide a practical simplified methodology for identifying the predominant failure mode of a pipe under reverse fault rupture. An extensive numerical parametric analysis is performed considering the main variables affecting the pipe response. Due to the nature of the topic and a large number of associated parameters, it is not straightforward to obtain strict criteria on whether a pipeline will buckle locally or globally. Instead, the aim is to provide pipe designers and operators with a handy tool for the preliminary assessment of the predominant failure mode of the pipe at hand, given the assumptions made and the pertinent numerical and statistical uncertainties.

2. Pipeline failure modes and verification criteria

Pipeline failure due to tensile fracture or local buckling is examined by comparing the code-based strain limits to the maximum longitudinal strain developed in the pipeline, while upheaval buckling is evaluated by examining whether the pipeline is exposed on the ground surface or not. The failure criteria for tensile fracture and local buckling are adopted from ALA [6] and EN1998-4 [5], which are two major international codes addressing the issue of the design of buried pipelines against seismic-induced permanent ground displacements. Even though there can be a lot of discussion on these criteria, herein, the relevant code-based criteria are adopted because a practical application is targeted and consequently the criteria are considered as reliable and conforming to current international practice.

2.1 Tensile fracture

The significant pipe bending caused by reverse faulting may lead to tensile fracture at weld locations. Code-based tensile strain limits aiming at preventing this failure mode are the following:

- ALA Guidelines for the Design of Buried Steel Pipe [6]

  Operable limit state:

$$\varepsilon_t^{\mathrm{ALA,oper}} = 2\% \tag{1}$$

  Pressure integrity limit state:

$$\varepsilon_t^{\mathrm{ALA,int}} = 4\% \tag{2}$$

- EN 1998-4 Silos, Tanks and Pipelines [5]:

$$\varepsilon_t^{\mathrm{EN\ 1998\text{-}4}} = 3\% \tag{3}$$

2.2 Local buckling

High compressive strains may lead to wrinkling that extends over a short pipe length and neither interrupts fuel flow nor allows a leak. The subsequent increase of compression may then lead to the evolvement of the wrinkle to a local buckle. Local buckling occurrence is also recognized as a sign of the pipe degrading capacity to resist other loads and thus codes provide expressions for limiting compressive strains below a maximum value:

- ALA Guidelines for the Design of Buried Steel Pipe [6]

  Operable limit state:

$$\varepsilon_c^{\text{ALA,oper}} = 0.50\left(\frac{t}{D'}\right) - 0.0025 + 3000\left(\frac{pD}{2Et}\right)^2, \text{ with } D' = D/(1 - 3\frac{D - D_{min}}{D}) \quad (4)$$

  Pressure integrity limit state:

$$\varepsilon_c^{\text{ALA,int}} = 1.76\frac{t}{D} \quad (5)$$

  where D is the pipe diameter, t is the pipe wall thickness, p is the pipe internal pressure, E is the pipeline steel modulus of elasticity and D_{min} is the pipe minimum diameter due to possible cross-section ovalization.

- EN 1998-4 Silos, Tanks and Pipelines [5]:

$$\varepsilon_c^{\text{EN 1998-4}} = \min\left\{1\%; 40\frac{t}{D}(\%)\right\} \quad (6)$$

  where D is the pipe diameter and t is the pipe wall thickness.

2.3 Upheaval buckling

Pertinent codes do not provide specific recommendations or expressions for the protection of onshore pipes against upheaval buckling. The only regulatory provision is par. C.6.3.3.5 of CSA Z662 [7], stating that the pipeline has to be designed in order to prevent upheaval buckling, whereas this case would be harmful to the pipeline. Upheaval buckling is therein defined as exposure of the pipeline on the ground surface [29],[37],[40]. Naturally, the definition of upheaval buckling occurrence can be a significant issue. Considering failure to occur a few centimeters below the ground surface, e.g. 10cm or 20cm, would change the results. Still, small changes are more pronounced for small diameter and shallowly buried pipes and are generally less significant than crossing geometry issues as discussed in Section 4.7.

The upheaval buckling occurrence is assessed in the present study in accordance with CSA Z662 [7]. Two successive stages of pipeline deformation are plotted in Figure 2. The first step presents the case of pipeline deformation without upheaval buckling, while the second step presents the case of upheaval buckling, i.e. the pipe is exposed on the ground surface. The pipeline top crown is located at depth H below the ground surface, Δf is the vertical fault offset magnitude, Δp is the maximum pipeline vertical displacement, $\delta\Delta$ is the pipeline relative vertical displacement in the soil and ψ is the fault dip angle. The pipe exposure on the ground surface is checked via $\delta\Delta$. For $\delta\Delta \leq H$ the pipe is not exposed, while for $\delta\Delta > H$ the pipe is considered to having been subjected to upheaval buckling.

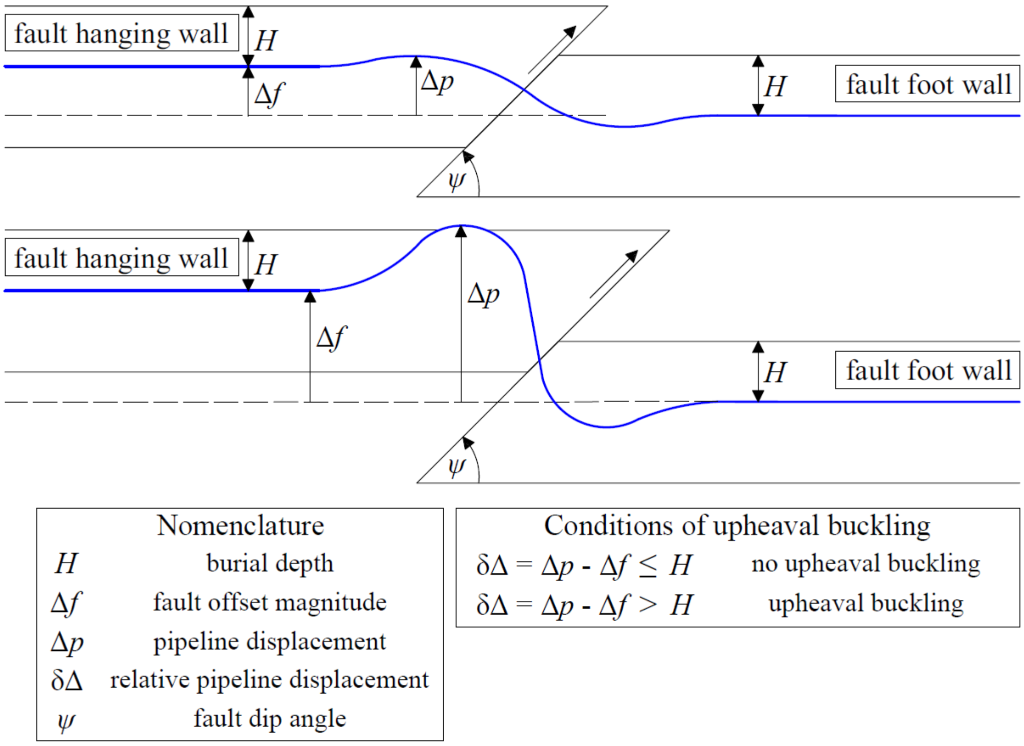

Figure 2: Assessment of pipeline upheaval buckling due to reverse faulting

3. Pipeline numerical model

A beam-type model is developed for the numerical analysis of the pipeline – reverse fault crossing (Figure 1) by employing the commercial software ADINA [47], following the provisions of ALA [6] and the numerical considerations discussed in [14],[34],[48]-[50]. The reliability of the numerical modeling and analysis has been verified by the authors by means of comparison to experimental results, in their previously published work ([49],[50]). Additionally, it is noted that the beam-type model for buried pipelines is the one recommended by all major international codes (ALA [6], EN1998-4 [5], CSA Z662 [7]) and the results of such models and analyses are routinely applied in practice for all major buried pipeline projects.

The developed model is schematically shown in Figure 3. The examined pipelines within the parametric analysis feature varying crossing-section in terms of diameter and thickness and varying steel grade, as described in Section 4. A straight pipeline segment with length equal to 1500m is examined, as good engineering practice and pertinent code provisions suggest to avoid route changes in fault crossing areas because bends might act as anchor points and introduce additional undesirable forces to the pipeline. The modeling length has been found from appropriate sensitivity analysis to be sufficient for the effects of PGDs to vanish. The pipe is meshed into PIPE elements, which are two-node Hermitian beam elements with extra degrees-of-freedom (DOFs) to account for the strains caused by in- (3 additional DOFs) and out-of-plane (3 additional DOFs) cross-section ovalization. The ovalization degrees of freedom are based on the von Karman ovalization modes [51]-[52]. Strains are calculated at several Gauss integration points on the pipe cross-section, namely 2 points along the element's longitudinal axis, 2 nodes through the cross-section thickness and 24 nodes along the circumference of the cross-section. Tensile fracture and local buckling are checked by comparing the code-based strain limit to the maximum longitudinal strain developed in the pipeline, regardless of the position of the maximum strain, while upheaval buckling is checked as per Section 2.3.

Two zones are defined along the pipe longitudinal direction, in which different mesh densities are employed: Zone 1 around the fault crossing and Zone 2 outside Zone 1. This differentiation has been adopted to achieve a balance between the reliability of results and the minimization of solution time and computational power. After carrying out a parametric study, the length of Zone 1 has been set equal to 150m with mesh density equal to 0.25m. The total length of Zone 2 equals 1,350m consisting of two parts with length equal to 675m each, with mesh density equal to 1m. In total, the pipe is meshed into 1,800 PIPE elements. The pipe steel material nonlinearity is addressed using a bi-linear stress-strain relationship, considering that the conditions of par. C.5.7.1 of CSA Z662 [7] are met, namely the examined pipe is hot-reduced electric welded with a diameter lower than 941mm (36in). Using a smoother steel stress-strain relationship (e.g. Ramberg-Osgood) would have been appropriate when examining local phenomena (e.g. in a shell model), but it makes a negligible difference in the global behavior of the model, as has been verified by comparing sample results with the two models. Finally, geometrical nonlinearity (large displacement formulation) is taken into consideration to account for the second-order effects, which alter both the peak strain values and the strain distribution along the pipeline.

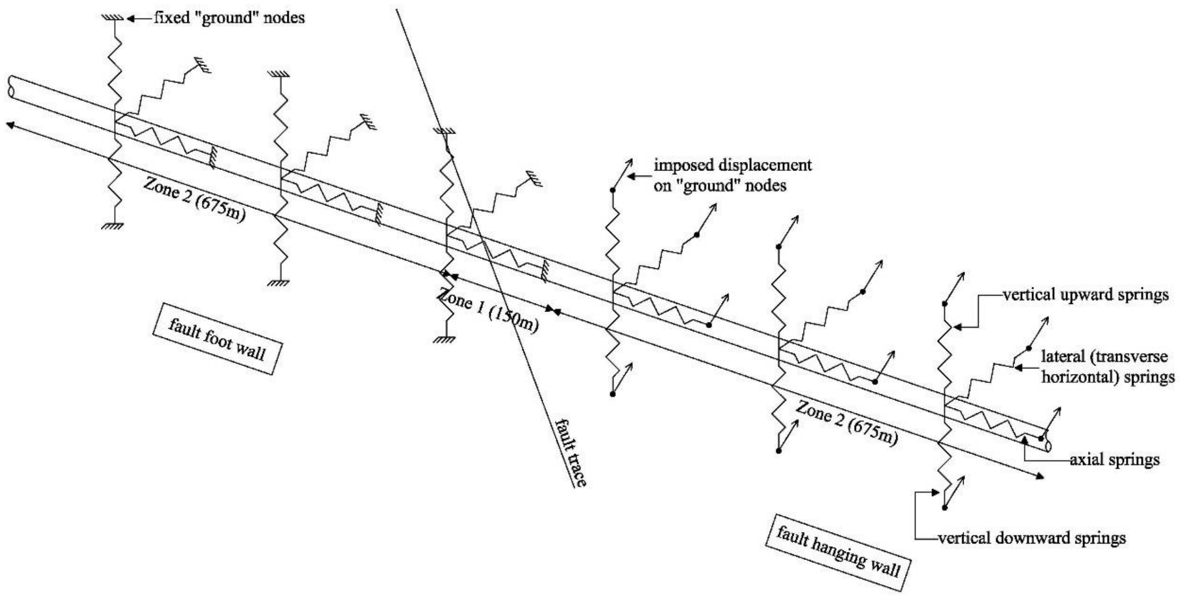

Figure 3: Schematic illustration of the developed pipeline – fault crossing beam-type numerical model

Fuel transmission pipelines are typically embedded within a trench that is assumed to be wide enough for the development of soil failure surfaces. Herein, the surrounding soil is modeled with mutually independent, nonlinear translational springs in four directions connect pipe nodes to “ground nodes”. Hence, every pipe node is supported by a set of four springs: (1) axial springs, which are orientated along the longitudinal pipe axis, model the pipe-soil friction, (2) lateral (transverse horizontal) springs model the soil resistance to pipe lateral movement in the trench with mechanisms similar to those of vertical anchor plates of horizontally moving foundations by activating passive earth pressure, (3) vertical upward springs model the backfill soil resistance to pipe movement towards the ground surface with the corresponding maximum force being equal to the weight of an inverted triangle prism of soil above the pipeline top and (4) vertical downward springs model the soil resistance to pipe movement towards the trench bottom with the corresponding soil forces acting on the pipe bottom being similar to those of the vertical bearing capacity of a footing. For downward movement, one should consider the native soil properties, but as it will be discussed in Section 4.7, soil properties play a rather minor role in the prediction of the predominant pipe failure mode, compared to fault crossing geometry. Soil springs' properties are estimated after ALA [6] provisions. In more detail:

- Axial springs

  The maximum axial soil force (T_u) per unit length of pipe is estimated via the expression:

$$T_u = \pi D a c + \pi D H \bar{\gamma} \frac{1 + K_o}{2} \tan \delta \tag{7}$$

  where D is the pipe outside diameter, c is the soil cohesion representative of the soil backfill, H is the depth to pipe centerline, $\bar{\gamma}$ is the effective unit weight of soil, K_o is the coefficient of pressure at rest, a is the adhesion factor, and δ is the interface angle of friction for pipe and soil that depends on the internal friction angle of the soil and the type of coating of the pipe.

  The maximum displacement depends on the soil type.

- Lateral springs

  The maximum lateral soil force (P_u) per unit length of pipe is estimated as:

$$P_u = N_{ch} c D + N_{qh} \bar{\gamma} H D \tag{8}$$

  where N_{ch} is the horizontal bearing capacity factor for clay, and N_{qh} is the horizontal bearing capacity factor.

  The maximum displacement in the lateral direction is a linear function of burial depth (H) and pipe diameter (D).

- Vertical upward springs

  The maximum vertical uplift soil force (Q_u) per unit length of pipe is estimated via the following expression:

$$Q_u = N_{cv} c D + N_{qv} \bar{\gamma} H D \tag{9}$$

  where N_{cv} is the vertical uplift factor for clay, and N_{qv} is the vertical uplift factor for sand.

  The maximum displacement in the vertical upward direction is a linear function of burial depth (H) and depends on pipe diameter (D) and soil type.

- Vertical downward springs

  The maxumum vertical bearing (downward) soil force (Q_d) per unit length of pipe is estimated as:

$$Q_u = N_{cv} c D + N_{qv} \bar{\gamma} H D \tag{10}$$

  where N_c, N_q, and N_γ are bearing capacity factors, γ is the totwl unit weight of soil.

  The maximum displacement in the vertical downward direction is a linear function of pipe diameter (D) and depends on the soil cohesion.

Soil springs are modeled in ADINA [47] using elastic-perfectly plastic SPRING elements (1801 elements in each direction) that exhibit stiffness only in the local axial direction. Soil spring properties depend on the pipe cross-section and the surrounding soil that are variables of the parametric study, as presented in Section 4. Herein, soil "ground nodes" located on the fault foot-wall are considered fixed, whilst the corresponding ones on the fault hanging wall are subjected to the imposed displacement caused by the fault offset. For numerical reasons, rotational degrees-of-freedom of "ground nodes" are fixed. The model consists of 9005 nodes in total.

The problem's inherent material and geometrical nonlinearity are handled through the implementation of the Newton-Raphson iterative solution algorithm with a sufficient number of analysis steps (1000 steps) to achieve numerical convergence. The energy convergence criterion is implemented with zero tolerance and the maximum number of iterations within a time step is 15. Moreover, the automatic time stepping (ATS) option of ADINA [47] is selected to achieve convergence in less solution time. The algorithm automatically sub-divides the load step until convergence is reached, while the time step might also be increased to accelerate the solution time. Apparently, the employment of the rigorous continuum numerical model (3D soil and pipe modeling with contact elements for pipe – soil interaction) could yield better predictions of the pipe failure, but at the cost of severely limiting the parameter exploration range, which tilted the choice in favor of the beam-type model adopted. As a final remark, non-seismic and in-service actions, such as internal pressure, corrosion, and hydraulic actions, are not considered in the present study.

4. Methodology and results

4.1 Range of parameters

The parameters considered as predictors of the predominant failure mode are:

- pipe – fault crossing geometry (Figure 1): fault dip angle ψ and pipe – fault crossing angle β,
- burial depth H (Figure 2),
- diameter to thickness (D/t) ratio,
- steel grade,
- soil properties (unit weight γ, cohesion c, and internal friction angle φ).

Investigated parameters values for pipe – fault crossing geometry and burial depth are listed in Table 1. The examined values of diameter to thickness (D/t) ratio are commercial ones and are listed in Table 2. The uncertainties of D/t ratios are not considered because it is assumed that the values are within the corresponding tolerances of API Specification 5L [53] and the examined parameters of the problem (fault crossing geometry, steel grade, soil type) have significant impact on the definition of the three areas in the "D/t ratio – burial depth" space, rather a minor variation of the D/t ratio. Preliminary numerical results have shown that pipes with diameter $D > 711\text{mm}\ (28\text{in})$ fail always due to local buckling, irrespective of wall thickness, burial depth and code-based strain limits adopted. Therefore, higher diameter values are not examined. The examined API steel grades [53] are tabulated in Table 3.

Table 1: Parameters for pipe – fault crossing geometry and burial depth

Parameter	Parameter name	Minimum	Maximum	Step
ψ	fault dip angle	30^{o}	90^{o}	10^{o}
β	pipe – fault crossing angle	30^{o}	80^{o}	10^{o}
H/D	normalized burial depth	1.00	3.60	0.20

Table 2: Commercial values of D/t ratio under examination

Pipe	D (mm)	t (mm)	D/t
6in	168.30	7.11	23.67
		10.97	15.34
		14.27	11.79
		18.26	9.22
		21.95	7.67
8in	219.10	6.35	34.50
		7.04	31.12
		8.18	26.78
		10.31	21.25
		12.70	17.25
		15.09	14.52
		18.26	12.00
		20.62	10.63
		22.23	9.86
10in	273.10	6.35	43.01
		7.80	35.01
		9.27	29.46
		12.70	21.50
		15.09	18.10
		18.26	14.96
		21.44	12.74
		25.40	10.75
		28.58	9.56
12in	323.90	6.35	51.01
		9.53	33.99
		12.70	25.50
		17.48	18.53
		25.40	12.75
		33.32	9.72

Pipe	D (mm)	t (mm)	D/t
16in	406.40	6.35	64.00
		9.53	42.64
		12.70	32.00
		16.66	24.39
		26.19	15.52
		30.96	13.13
		40.49	10.04
20in	508.00	6.53	77.79
		12.70	40.00
		20.62	24.64
		32.54	15.61
		44.45	11.43
		50.01	10.16
		6.53	77.79
24in	610.00	6.35	96.06
		12.70	48.03
		17.48	34.90
		30.96	19.70
		46.02	13.26
		59.54	10.25
28in	711.00	7.92	89.77
		9.53	74.61
		12.70	55.98
		15.88	44.77

Table 3: API 5L steel grades under consideration

Steel grade	Yield stress (MPa)	Ultimate stress (MPa)
X52	359.0	455.0
X56	386.5	489.5
X60	414.0	517.5
X65	448.5	531.0
X70	483.0	565.5
X80	555.0	621.0
X100	690.0	760.0

Pipe – soil interaction dominates the pipe response and thus it is suggested by constructional practice and code provisions to backfill the trench with granular soil in order to minimize the soil resistance to pipe movement in the trench. Accordingly, three indicative cohesionless soils are examined (Table 4), excluding cohesive (clay) soil types.

Table 4: Soil types under consideration

Soil type	Friction angle	Unit weight (kN/m^3)
Loose sand	30^o	16.0
Medium sand	33.5^o	17.9
Dense sand	40^o	20.0

4.2 Methodology outline

An indicative case of fault crossing geometry is examined at first in order to demonstrate the process of deriving the proposed simplified expressions. A typical API 5L X65 (Table 3) pipeline is examined, buried in medium sand (Table 4) and crossing a reverse fault with dip angle ψ = 40^o at a crossing angle β = 60^o. The pipeline is numerically analyzed for all combinations of burial depths (Table 1) and D/t ratios (Table 2). Results are presented in the "D/t ratio – burial depth" space (Figure 4a), considering the operable limits of ALA (Section 2). Each point comes from a single pipeline analysis and it is appropriately marked to indicate the predominant pipe failure mode. It is observed that in the upper-right side (high burial depth and D/t ratio) the pipe fails due to local buckling, while in the lower-left side (low burial depth and D/t value) the pipe fails due to upheaval buckling, as qualitatively predicted in [4]. There is, also, an intermediate area between the two previously described ones, where a small change of a parameter might trigger a different predominant failure mode, highlighting the sensitivity of the problem to the parameters.

A first attempt to delimit the failure mode areas in the "D/t ratio – burial depth" space is performed by employing Linear Discriminant Analysis (LDA) [54]. LDA is a classification method that is applied when groups are known a priori. The LDA curve, shown in Figure 4(b), stands as a preliminary index for the quantification of the Yun and Kyriakides [4] criterion but has limited practical applicability due to the above mentioned high sensitivity to parameters in the intermediate area. To that effect, two additional limits, are introduced, namely the 0% local buckling and the 100% local buckling (Figure 4b). The 0% local buckling limit line is generated by parallel displacement of the LDA line towards lower values of *D*/*t* ratio and depth *H* until all local buckling points are above and to its right. Similarly, the 100% local buckling limit line is generated by parallel displacement of the LDA line towards higher values of *D*/*t* ratio and depth *H* until all local buckling points are below and to its left. For pipeline designs located to the right and above the 100% local buckling limit, the pipe is expected always to fail due to local buckling, while for pipeline designs located to the left and below the 0% local buckling limit, the pipe is expected always to fail due to upheaval buckling or tensile fracture, depending on the adopted code-based strain limits and the design parameters. Between these two extremes, the LDA line provides a single "optimal" division of the intermediate area. The process outlined above is schematically portrayed in Figure 5.

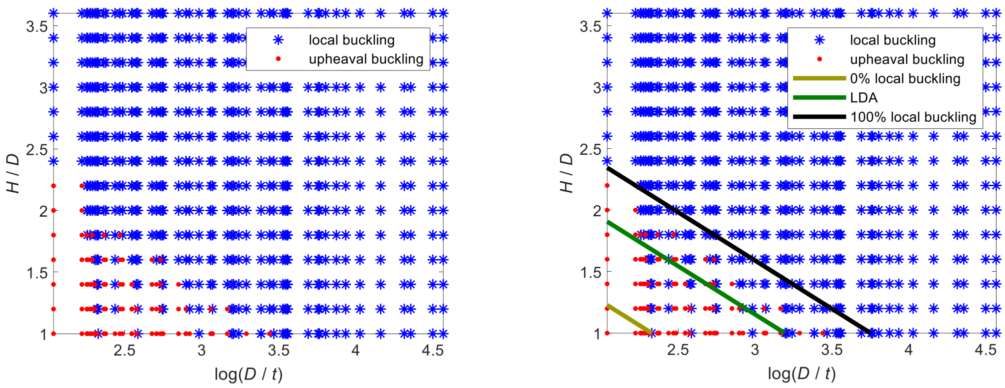

(a) (b)

Figure 4: (a) Predominant failure mode of an API X65 pipeline buried in medium sand for fault dip angle ψ = 40° and crossing angle β = 60°, (b) LDA, 0% local buckling and 100% local buckling lines in the "*D*/*t* ratio – burial depth" space

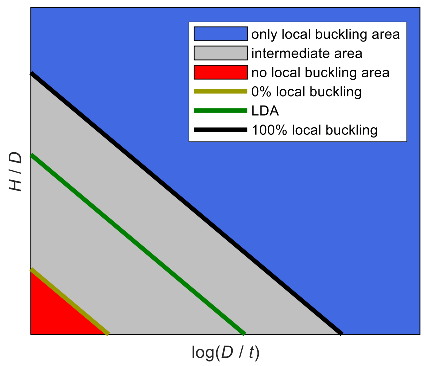

Figure 5: Schematic illustration of the predominant pipe failure modes in the "*D*/*t* ratio – burial depth" space

The 0% local buckling, LDA, and 100% local buckling lines are estimated via the expressions:

$$Det_0 = A_0 \log\left(\frac{D}{t}\right) + B_0\left(\frac{H}{D}\right) + 1 = 0 \quad (11)$$

$$Det_{LDA} = A_{LDA} \log\left(\frac{D}{t}\right) + B_{LDA}\left(\frac{H}{D}\right) + 1 = 0 \quad (12)$$

$$Det_{100} = A_{100} \log\left(\frac{D}{t}\right) + B_{100}\left(\frac{H}{D}\right) + 1 = 0 \tag{13}$$

where A_0, B_0, A_{LDA}, B_{LDA}, A_{100}, B_{100} are the coefficients that depend on the pipe – fault crossing geometry, steel grade, and soil type. Specifically, the coefficients are assumed to be linear combinations of three functions of the problem parameters:

$$\begin{cases} A_0 = p_1 G_{A,0}(\psi,\beta) + p_2 ST_{A,0}(F_y) + p_3 S_{A,0}(soil\ type) \\ A_{\text{LDA}} = p_1 G_{A,\text{LDA}}(\psi,\beta) + p_2 ST_{A,\text{LDA}}(F_y) + p_3 S_{A,\text{LDA}}(soil\ type) \\ A_{100} = p_1 G_{A,100}(\psi,\beta) + p_2 ST_{A,100}(F_y) + p_3 S_{A,100}(soil\ type) \end{cases} \tag{14}$$

$$\begin{cases} B_0 = p_1 G_{B,0}(\psi,\beta) + p_2 ST_{B,0}(F_y) + p_3 S_{B,0}(soil\ type) \\ B_{\text{LDA}} = p_1 G_{B,\text{LDA}}(\psi,\beta) + p_2 ST_{B,\text{LDA}}(F_y) + p_3 S_{B,\text{LDA}}(soil\ type) \\ B_{100} = p_1 G_{B,100}(\psi,\beta) + p_2 ST_{B,100}(F_y) + p_3 S_{B,100}(soil\ type) \end{cases} \tag{15}$$

where:

$G(\psi,\beta)$	:	function to consider the effect of crossing geometry with fault dip angle ψ and pipe – fault crossing angle β (Section 4.3)
$ST(F_y)$	:	function to consider the effect of steel grade. $F_y = f_y/448.50$, where f_y is the steel yield stress in MPa and 448.50MPa is the yield stress of the reference grade X65 (Section 4.4)
$S(soil\ type)$	:	function to consider the effect of soil type (Section 4.5)
p_1	:	coefficient for the effect of crossing geometry
p_2	:	coefficient for the effect of steel grade
p_3	:	coefficient for the effect of soil type

Fault crossing geometry is considered to have a primary effect on the prediction of the predominant failure mode of the pipeline. Thus, in terms of design of numerical experiments [55], crossing geometry is treated as a full functional design, examining all possible combinations of angles ψ and β in order to study the effect of each angle (parameter or factor) on the predominant failure mode (response variable), as well as the effect of interactions between factors on the response variable.

On the other hand, steel grade and soil type are treated as secondary effects and consequently, there is no full exploration of their influence. Hence, a central value is examined, and the effect of steel grade and soil type is investigated by considering only a single "mean crossing geometry" with $\psi = 60^o$ and $\beta = 60^o$. In summary, the effect of crossing geometry is firstly examined by considering all possible combinations of angles (ψ,β) and then the steel grade and soil type effects are added, without considering interactions, via the linear combination of Eqs. (14) and (19) with the appropriate coefficients p_1, p_2, and p_3.

Overall, the methodology followed to fit Eqs. (11) through (13) is outlined below and is applied for each adopted code:

1. Estimate the predominant failure mode for all 7×6 combination of angles β and ψ (Table 1) for X65 steel grade and medium sand times 751 combinations of D/t ratio and burial depth H resulting to $7 \times 6 \times 751$ analyses (Section 4.3)
2. Estimate the predominant failure mode for $\psi = 60^o$ and $\beta = 60^o$, medium sand soil, and all 7 steel grades (Table 3) resulting to 7×751 analyses (Section 4.4)

3 Estimate the predominant failure mode for ψ = 60º and β = 60º, X65 steel grade and all three soil types (Table 4) resulting to 3×751 analyses (Section 4.5)

4 Fit Eqs. (11) through (13) in each of the $7\times 6+7+3$ realizations of the "D/t ratio – burial depth" space to generically determine the coefficients (A_0, B_0), (A_{LDA}, B_{LDA}), (A_{100}, B_{100})

5 Use the 7×6 geometry realizations to fit generic function $G(\psi,\beta)$ for each of the three A and B coefficients (Section 4.3) [note that A is A_0, A_{LDA}, A_{100}, and B is B_0, B_{LDA}, B_{100}]

6 Use the 7 steel grades realizations to fit general function $ST(F_y)$ for each of the A and B coefficients (Section 4.4)

7 Use the 3 soil type realization to fit the general function S(*soil type*) for each of the A and B coefficients (Section 4.5)

8 Use direct search to optimize the linear combination coefficients p_1, p_2, and p_3 for Eqs. (14) and (19) to best predict A and B for all $7\times 6+7+3$ realizations (Section 4.7)

9 Validate the fitted equations on a test set different from the training set (Section 4.8)

4.3 Effect of pipe – fault crossing geometry

Pipe – fault crossing geometry is the primary parameter affecting pipe mechanical behavior. Indicative results for an API X65 pipeline, buried in medium sand with fault crossing angles ψ = 30º and β = 70º are presented in Figure 6, considering ALA operable strain limits, ALA pressure integrity strain limits and EN 1998-4 strain limits (Section 2). In general, for a given crossing angle β, steel grade, and soil type, increasing the fault dip angle ψ leads to increased pipe bending and consequently a larger "area" (i.e. more D/t ratio and burial depth combinations) of local buckling occurrence. This becomes apparent both for 0% and 100% local buckling limits (Figure 7) pulling them up and to the right when ψ increases. On the other hand, keeping everything else constant, the crossing angle β has a non-negligible yet considerably lower influence on the limits (Figure 8).

The adopted code-based strain limits play an important role in the critical failure mode. In the case of adopting the ALA pressure integrity strain limits [Figure 6(b)], the compressive strain limit is higher than the other code-based limits and consequently, significantly more points of tensile fracture are observed.

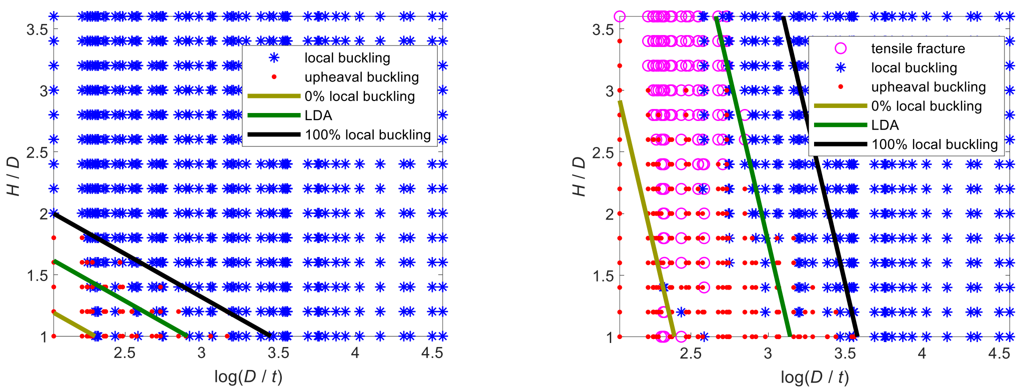

(a) (b)

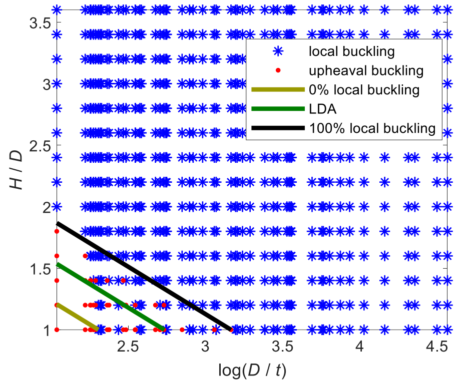

(c)

Figure 6: Predominant failure mode of API X65 pipeline, buried in medium sand with crossing geometry ψ = 30° and β = 70° adopting (a) ALA operable limits, (b) ALA pressure integrity limits, (c) EN 1998-4 limits

The effect of fault crossing geometry is incorporated in the limit lines in Eqs. (14) and (15) via the general function $G(\psi,\beta)$:

$$G(\psi,\beta) = g_1 + g_2\beta + g_3\psi + g_4\beta\psi + g_5\psi^2 + g_6\beta\psi^2 + g_7\psi^3 \qquad (16)$$

where $g_1, g_2,\ldots,g_7$ are the fitting coefficients. Evidently, to accommodate all observations on the relative significance of ψ and β, angle ψ is captured with terms up to the third power, while for angle β only linear terms are employed, including all interaction terms up to the third order. The resulting fitting coefficients are listed in Table 5 for ALA operable limits, in Table 6 for ALA pressure integrity limits and in Table 7 for EN 1998-4 limits. Indicative results of the fitted surfaces for coefficients A_0 and B_0 considering ALA operable strain limits are depicted in Figure 9. As expected, higher fidelity is achieved in the middle of the training set, compared to its edges. Moreover, it has to be noted that the case of fault dip angle ψ = 90° has not been considered in this parametric study because a reliable distinction of failure modes cannot be performed in the "D/t ratio – burial depth" space (Figure 10). In this case, the intermediate area is very extended, rendering the identification of the predominant failure mode impractical.

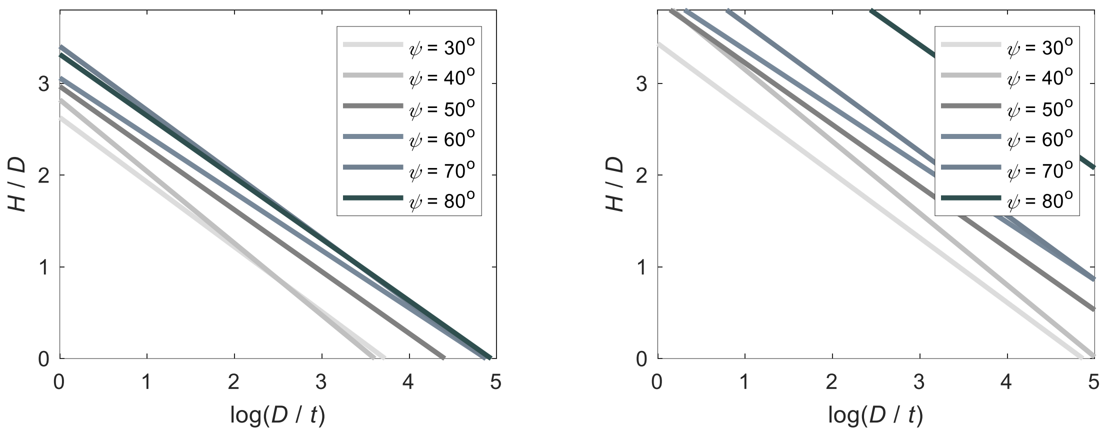

(a) (b)

Figure 7: Effect of fault dip angle for constant crossing angle β = 70°, considering ALA operable limits: variation of (a) 0% local buckling and (b) 100% local buckling limits

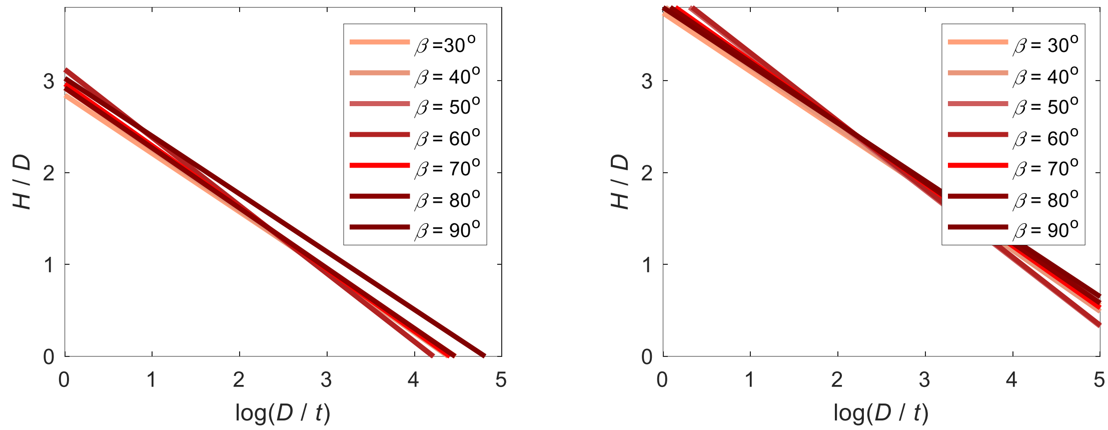

(a) (b)

Figure 8: Effect of crossing angle for constant fault dip angle ψ = 50°, considering ALA operable limits: variation of (a) 0% local buckling and (b) 100% local buckling limits

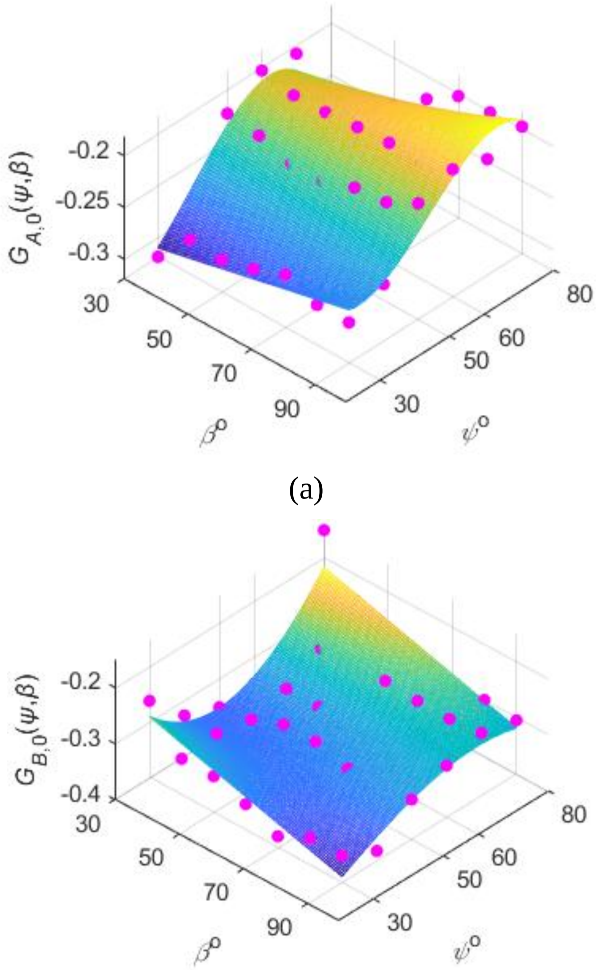

(b)

Figure 9: 3D surface fitting for considering the effect of fault crossing geometry in order to obtain the coefficients (API X65 pipeline buried in medium sand)

Table 5: ALA operable strain limits: Coefficients for considering the effect of fault crossing geometry

Limit curve		Coefficients for Eq. (16) $G(\psi,\beta) = g_1 + g_2\beta + g_3\psi + g_4\beta\psi + g_5\psi^2 + g_6\beta\psi^2 + g_7\psi^3$						
		g_1	g_2	g_3	g_4	g_5	g_6	g_7
0% local buckling	$G_{A,0}$	-0.3954	0.0044	-0.0036	-1.7412×10^{-4}	2.6983×10^{-4}	1.7353×10^{-6}	-2.6839×10^{-6}
	$G_{B,0}$	0.3846	-0.0098	-0.0306	3.7314×10^{-4}	3.3798×10^{-4}	-3.3943×10^{-6}	-5.2753×10^{-7}
LDA	$G_{A,LDA}$	-0.6267	0.0047	0.0122	-1.6702×10^{-4}	-4.0737×10^{-5}	1.5210×10^{-6}	-6.8061×10^{-7}
	$G_{B,LDA}$	0.0043	-0.0075	-0.0084	3.0634×10^{-4}	-3.5935×10^{-5}	-2.9234×10^{-6}	1.5153×10^{-6}
100% local buckling	$G_{A,100}$	-0.6400	0.0048	0.0153	-1.7852×10^{-4}	-1.1441×10^{-4}	1.6052×10^{-6}	-1.0307×10^{-7}
	$G_{B,100}$	-0.1338	-0.0049	-7.0187×10^{-4}	1.9316×10^{-4}	-1.2752×10^{-4}	-1.8593×10^{-6}	1.8027×10^{-6}

Table 6: ALA pressure integrity strain limits: Coefficients for considering the effect of fault crossing geometry

Limit curve		Coefficients for Eq. (16) $G(\psi,\beta) = g_1 + g_2\beta + g_3\psi + g_4\beta\psi + g_5\psi^2 + g_6\beta\psi^2 + g_7\psi^3$						
		g_1	g_2	g_3	g_4	g_5	g_6	g_7
0% local buckling	$G_{A,0}$	-0.9130	0.0038	0.0199	-1.3307×10^{-4}	-1.2907×10^{-4}	1.2069×10^{-6}	-4.7461×10^{-7}
	$G_{B,0}$	-0.2279	-0.0047	0.0220	1.3940×10^{-4}	-5.9792×10^{-4}	-7.8476×10^{-7}	4.1277×10^{-6}
LDA	$G_{A,LDA}$	-0.4134	0.0022	-6.2682×10^{-4}	-5.5855×10^{-5}	1.2032×10^{-4}	2.8827×10^{-7}	-1.0347×10^{-6}
	$G_{B,LDA}$	-0.1582	-0.0040	0.0173	1.2326×10^{-4}	-4.9937×10^{-4}	-7.5973×10^{-7}	3.6018×10^{-6}
100% local buckling	$G_{A,100}$	-0.6856	0.0043	0.0153	-1.3892×10^{-4}	-1.1959×10^{-4}	9.8857×10^{-7}	6.2992×10^{-8}
	$G_{B,100}$	0.1575	-0.0024	0.0143	6.7121×10^{-5}	-3.8414×10^{-4}	-3.7401×10^{-7}	2.6890×10^{-6}

Table 7: EN 1998-4 strain limits: Coefficients for considering the effect of fault crossing geometry

Limit curve		Coefficients for Eq. (16) $G(\psi,\beta) = g_1 + g_2\beta + g_3\psi + g_4\beta\psi + g_5\psi^2 + g_6\beta\psi^2 + g_7\psi^3$						
		g_1	g_2	g_3	g_4	g_5	g_6	g_7
0% local buckling	$G_{A,0}$	-0.6272	0.0048	0.0091	-1.6529×10^{-4}	1.9910×10^{-5}	1.4529×10^{-6}	-9.2010×10^{-7}
	$G_{B,0}$	0.9514	-0.0131	-0.0582	4.7404×10^{-4}	7.7825×10^{-4}	-4.0458×10^{-6}	-3.0738×10^{-6}
LDA	$G_{A,LDA}$	-0.8472	0.0057	0.0223	-1.9114×10^{-4}	-2.0776×10^{-4}	1.6075×10^{-6}	3.5633×10^{-7}
	$G_{B,LDA}$	0.4905	-0.0099	-0.0337	3.6390×10^{-4}	4.0528×10^{-4}	-3.1424×10^{-6}	-1.2562×10^{-6}
100% local buckling	$G_{A,100}$	-0.7917	0.0052	0.0221	-1.7401×10^{-4}	-2.2553×10^{-4}	1.4552×10^{-6}	5.8575×10^{-7}
	$G_{B,100}$	0.3473	-0.0080	-0.0254	2.8810×10^{-4}	2.8805×10^{-4}	-2.4685×10^{-6}	-7.3335×10^{-7}

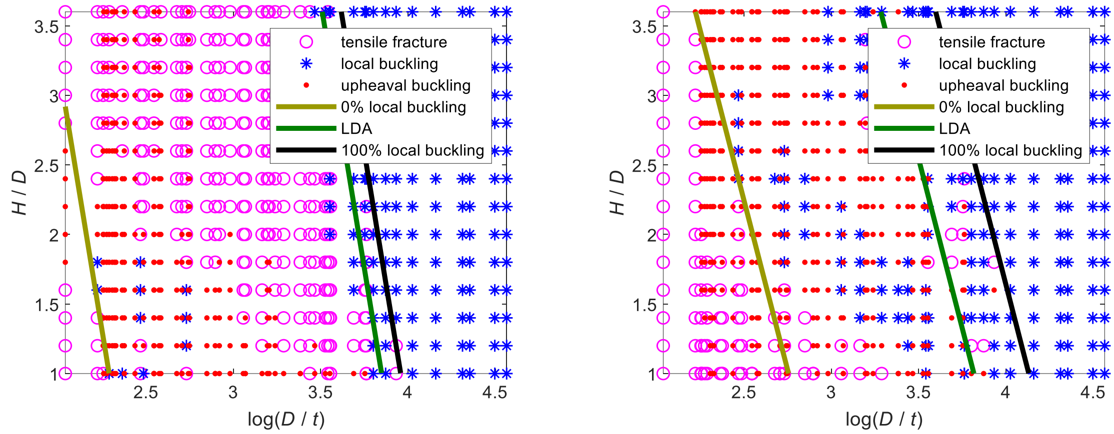

(a) (b)

Figure 10: Predominant failure mode API X65 pipeline, buried in medium sand with crossing geometry: (a) ψ = 90° and β = 30° adopting ALA operable strain limits, (b) ψ = 90° and β = 60° adopting EN 1998-4 strain limits

4.4 Effect of pipe steel grade

Pipeline steel grade properties affect the response of the pipeline under faulting and in particular the available ductility of the structure (indicatively [33],[56]). Pipelines buried in medium sand crossing a reverse fault with the "mean crossing geometry" (ψ = 60° and β = 60°) are examined. Steel grades under examination are listed in Table 3. Indicative results for X52, X70, and X100 pipes considering ALA operable limits are shown in Figure 11. It is observed that the increase of steel grade leads to a decrease in the local buckling "area" in the "*D*/*t* ratio – burial depth" space, while the intermediate area is roughly constant.

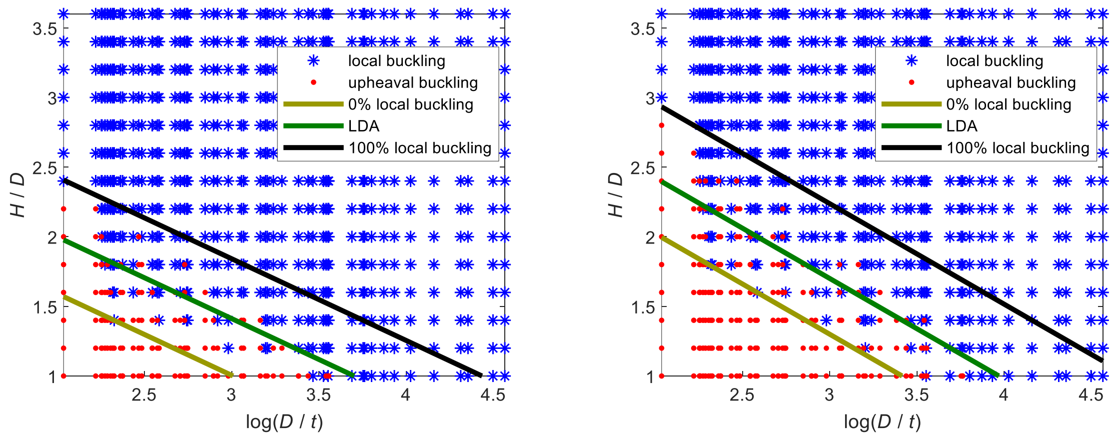

(a) (b)

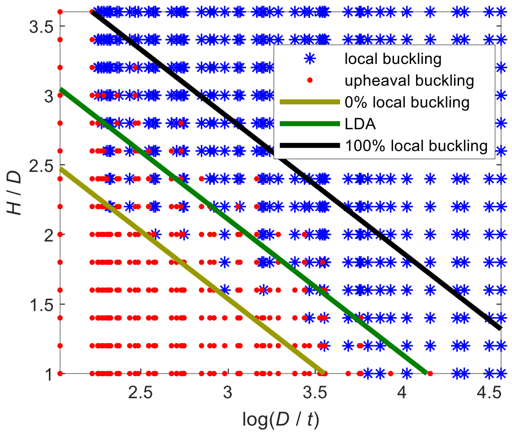

(c)

Figure 11: Predominant failure mode of pipelines buried in medium sand with fault crossing geometry ψ = 60° and β = 60°: (a) X52 pipe, (b) X70 pipe, and (c) X100 pipe, adopting ALA operable limits

Collecting all results for different steel grades, 2D curve fitting is performed to estimate the effect of steel grade through function $ST(F_y)$:

$$ST(F_y) = st_1 F_y^4 + st_2 F_y^3 + st_3 F_y^2 + st_4 F_y + st_5 \qquad (17)$$

where $F_y = f_y/448.50$ is the normalized yield stress (f_y in MPa) with respect to the yield stress of the reference X65 steel grade. The fitting coefficients st_1, st_2,…,st_5 are listed in Table 8 for ALA operable limits, in Table 9 for ALA pressure integrity limits, and in Table 10 for EN 1998-4 limits.

Table 8: ALA operable strain limits: Coefficients for considering the effect of steel grade

Limit curve		Coefficients for Eq. (17) $ST(F_y) = st_1 F_y^4 + st_2 F_y^3 + st_3 F_y^2 + st_4 F_y + st_5$				
		st_1	st_2	st_3	st_4	st_5
0% local buckling	$ST_{A,0}$	-0.0919	0.8270	-2.1427	2.1440	-0.9419
	$ST_{B,0}$	6.3355	-29.1165	49.1737	-35.9664	9.2522
LDA	$ST_{A,LDA}$	-1.6726	7.8756	-13.6803	10.3662	-3.0695
	$ST_{B,LDA}$	3.2219	-15.1980	25.7198	-18.9936	4.7893
100% local buckling	$ST_{A,100}$	-1.2909	6.1938	-10.9571	8.4451	-2.5491
	$ST_{B,100}$	3.0523	-14.0848	23.8720	-17.4577	4.3710

Table 9: ALA pressure integrity strain limits: Coefficients for considering the effect of steel grade

Limit curve		Coefficients for Eq. (17) $ST(F_y) = st_1F_y^4 + st_2F_y^3 + st_3F_y^2 + st_4F_y + st_5$				
		st_1	st_2	st_3	st_4	st_5
0% local buckling	$ST_{A,0}$	0.4618	-2.0470	3.3210	-2.3159	0.2942
	$ST_{B,0}$	-0.2713	1.4149	-2.7205	2.2737	-0.7809
LDA	$ST_{A,LDA}$	0.0124	-0.1135	0.2972	-0.2705	-0.1867
	$ST_{B,LDA}$	-0.3733	1.8307	-3.3232	2.6416	-0.8525
100% local buckling	$ST_{A,100}$	-0.6419	3.0554	-5.3738	4.1717	-1.4423
	$ST_{B,100}$	-0.5387	2.6246	-4.7307	3.7347	-1.1578

Table 10: EN 1998-4 strain limits: Coefficients for considering the effect of steel grade

Limit curve		Coefficients for Eq. (17) $ST(F_y) = st_1F_y^4 + st_2F_y^3 + st_3F_y^2 + st_4F_y + st_5$				
		st_1	st_2	st_3	st_4	st_5
0% local buckling	$ST_{A,0}$	-1.2409	5.8036	-10.0616	7.6455	-2.3428
	$ST_{B,0}$	3.2799	-15.4517	26.7639	-19.9763	5.0253
LDA	$ST_{A,LDA}$	-1.2864	6.0945	-10.6889	8.2046	-2.4941
	$ST_{B,LDA}$	2.4072	-11.2405	19.2890	-14.2255	3.4581
100% local buckling	$ST_{A,100}$	-1.2563	5.9674	-10.4895	8.0714	-2.4416
	$ST_{B,100}$	1.7962	-8.3530	14.2595	-10.4180	2.4436

4.5 Effect of soil properties

As already mentioned, soil properties are defined by their fundamental parameters, namely unit weight, internal friction angle, and cohesion. Considering that it is not practically feasible to examine all combinations of soil properties, three typical sandy soils are examined (Table 4). The evaluation of the effect of soil properties is carried out by investigating a typical API X65 pipe that crosses a reverse fault with the "mean crossing geometry" (ψ = 60° and β = 60°). Indicative results considering ALA operable limits for different soil types are shown in Figure 12. It is deduced that the increase of the sand internal friction leads to an increase of soil resistance to pipe movement in the trench and consequently of pipe – soil friction. Hence, the local buckling "area" "*D*/*t* ratio – burial depth" space is increased, while the intermediate area remains roughly constant.

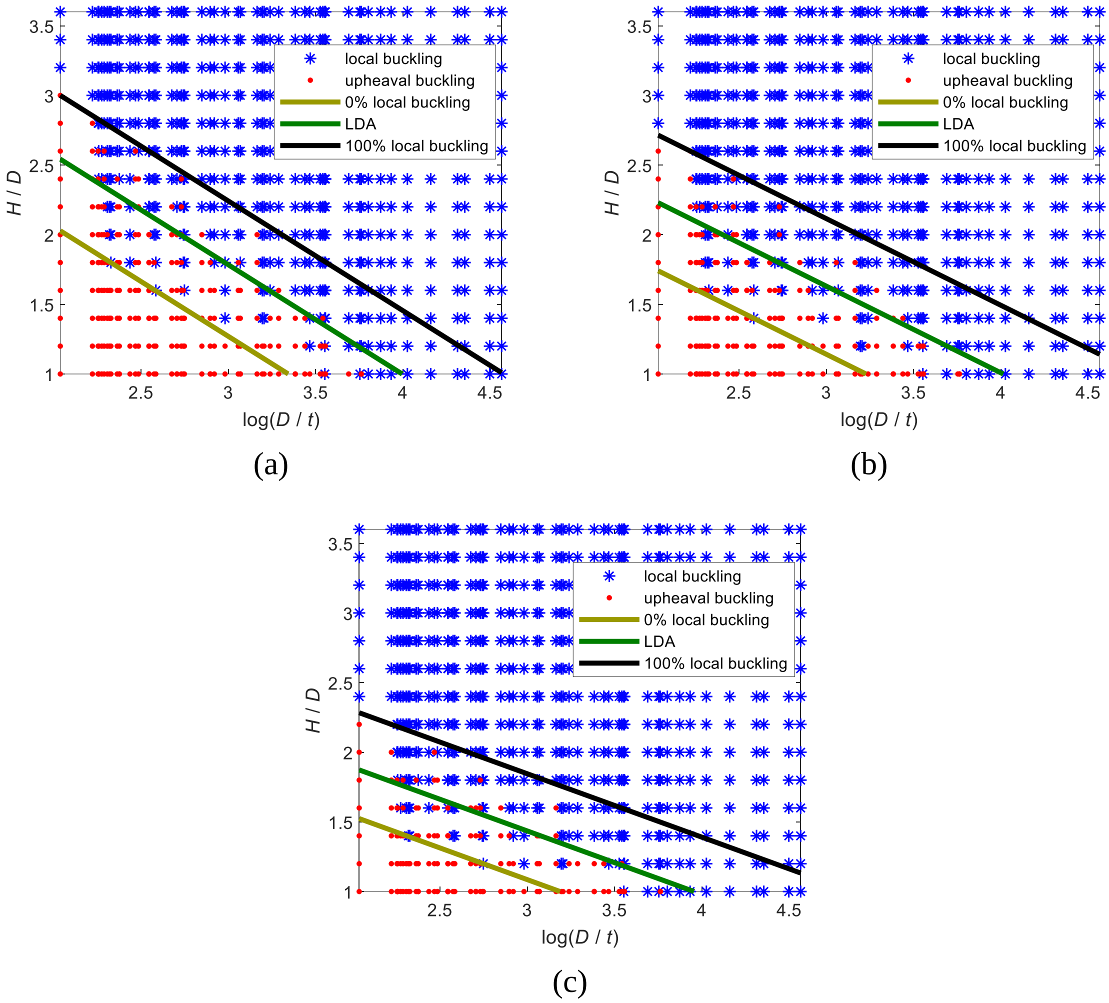

Figure 12: Predominant failure mode of API X65 pipeline with fault crossing geometry ψ = 60° and β = 60°) considering different soil types and adopting ALA operable limits: (a) loose sand, (b) medium sand, and (c) dense sand. Denser sands cause an anti-clockwise rotation of limit lines around a roughly constant rightmost corner.

The parameter of soil properties is treated as a categorical value and thereafter, function $S(\text{soil type})$ assumes constant values for each soil type, without more elaborate curve fitting. Corresponding fitted values of function $S(\text{soil type})$ are listed in Table 11 for ALA operable limits, Table 12 for ALA pressure integrity limits, and in Table 13 for EN 1998-4 limits.

Table 11: ALA operable strain limits: fitting values of function $S(\text{soil type})$ to account for the effect of soil type

Limit curve		Values of $S(\text{soil type})$ Loose sand	Medium sand	Dense sand
0% local buckling	$S_{A,0}$	-0.2168	-0.2069	-0.1857
	$S_{B,0}$	-0.2753	-0.3324	-0.4080
LDA	$S_{A,\mathrm{LDA}}$	-0.1899	-0.1780	-0.1626
	$S_{B,\mathrm{LDA}}$	-0.2412	-0.0286	-0.3571
100% local buckling	$S_{A,100}$	-0.1710	-0.1563	-0.1418
	$S_{B,100}$	-0.2172	-0.2511	-0.3114

Table 12: ALA pressure integrity strain limits: fitting values of function $S(\text{soil type})$ to account for the effect of soil type

Limit curve		Values of $S(\text{soil type})$ Loose sand	Medium sand	Dense sand
0% local buckling	$S_{A,0}$	-0.2811	-0.2849	-0.3060
	$S_{B,0}$	-0.0810	-0.0838	-0.0872
LDA	$S_{A,\mathrm{LDA}}$	-0.2572	-0.2601	-0.2713
	$S_{B,\mathrm{LDA}}$	-0.0741	-0.0766	-0.0773
100% local buckling	$S_{A,100}$	-0.2338	-0.2246	-0.2371
	$S_{B,100}$	-0.0673	-0.0661	-0.0676

Table 13: EN 1998-4 strain limits: fitting values of function $S(\text{soil type})$ to account for the effect of soil type

Limit curve		Values of $S(\text{soil type})$ Loose sand	Medium sand	Dense sand
0% local buckling	$S_{A,0}$	-0.2079	-0.1949	-0.1951
	$S_{B,0}$	-0.3169	-0.3545	-0.4372
LDA	$S_{A,\mathrm{LDA}}$	-0.1784	-0.1709	-0.1643
	$S_{B,\mathrm{LDA}}$	-0.2718	-0.3107	-0.3680
100% local buckling	$S_{A,100}$	-0.1586	-0.1478	-0.1436
	$S_{B,100}$	-0.2417	-0.2688	-0.3216

4.6 Classification of error metrics

In statistics literature [57], the nomenclature of classification errors is geared towards understanding medical test results. A positive outcome, thus, stands for evidence of having a given disease or condition. The following values are used to estimate metrics: *TP* (true positive) is the number of points predicted correctly, *TN* (true negative) is the number of points correctly discarded, *FP* (false positive) is the number of points incorrectly predicted and *FN* (false negative) is the number of points incorrectly rejected. Then, the three standard error metrics for classification are defined as:

$$\text{precision: } PR = \frac{TP}{TP+FP} \leq 1 \tag{18}$$

$$\text{recall: } RE = \frac{TP}{TP+FN} \leq 1 \tag{19}$$

$$\text{balanced accuracy: } BA = 1 - \frac{1}{2}\left[\frac{FN}{FN+TP} + \frac{FP}{FP+TN}\right] \leq 1 \tag{20}$$

The aforementioned error metrics can be better understood through an illustrative example. Suppose we have 20 points (15 local buckling points and 5 upheaval buckling points) in the "*D*/*t* ratio – burial depth" space indicating the predominant failure mode of a pipeline under reverse faulting. Following the procedure presented in section 4.2, the LDA line is drawn and local buckling points are considered to be a positive outcome of the LDA statistical model. The model identifies 10 local buckling points on the right-hand side of the LDA curve. However, it is observed that only 8 out of 10 points are actually local buckling ones, while the other 2 are misidentified as upheaval buckling points. In this case, we have $TP = 8$ (local buckling points correctly identified), $TN = 5 - 2 = 3$ (upheaval buckling points correctly identified), $FP = 2$ (upheaval buckling points incorrectly identified), and $FN = 15 - 8 = 7$ (local buckling points incorrectly identified). The precision after Eq. (18) is $PR = 8/(8+2) = 0.80$ and shows how useful the results are in predicting local buckling (if the model predicts local buckling, then 80% of the time it is correct). The recall after Eq. (19) is $RE = 8/(8+7) = 0.53$ and shows how complete the results are or in other words shows how many local buckling points have been identified out of their total number. Thus, the model was correct wherever it predicted the failure mode as local buckling, but it misidentified a lot of local buckling points as non-local buckling. In general, high precision reveals that the statistical model returned more correct results than incorrect, while high recall shows that most of the correct results have been identified. Then, balanced accuracy after Eq. (20) is $BA = 1 - 0.5[7/(7+8) + 2/(2+3)] = 0.87$, indicating that the overall performance of the classification process with LDA is 87%. Balanced accuracy checks the performance of the statistical model by overcoming the problem of unbalanced data through the normalization of *TP* and *TN* predictions by the number of positive and negative samples, respectively.

In statistical testing, a type I error is the false-positive finding, while a type II error is the false negative. In other sciences, such as medicine, the distinction between these two types of error is crucial, for example, in case of a disease, type I is preferred because the test might show that a healthy person has the disease, leading to re-testing, while type II error is not preferred as the test might show that an ill person is healthy. Differently, in the present study both type I and II errors have the same impact on the prediction of the predominant failure mode of the pipe. Thus, balanced accuracy is the appropriate metric to evaluate the overall performance of the model, namely the LDA line. Instead, in case of the 0% and 100% local buckling limits the interest is on having zero local buckling points on the left-hand side of the 0% local buckling limit and respectively zero non-local buckling points on the right-hand side of the 100% local buckling limit. Therefore, precision, where positive values stand for local buckling occurrence, is the appropriate error metric for the 100% local buckling limit, while the precision, where positive values stand for non-local-buckling occurrence, is the appropriate metric for the 0% local buckling limit. During the formulation of the full statistical model that takes into account all parameters, our concern is thus to minimize the number of local buckling points on the left-hand side of the 0% local buckling limit and respectively minimize the number of non-local-buckling points on the right-hand side of the 100% local buckling limit.

4.7 Combined effect of parameters

To combine the effects of all parameters into a single model, a direct search was employed to maximize the precision for 0% and 100% local buckling limits and the balanced accuracy for the LDA line over the entire training set. The resulting coefficients for Eqs. (14) and (15) are:

$$\begin{cases} p_1 = 0.80 \\ p_2 = 0.05 \\ p_3 = 0.15 \end{cases} \tag{21}$$

Then, the values of Eq. (21) are substituted in Eqs. (14) and (15) for estimating coefficients *A* and *B*:

$$\begin{cases} A_0 = 0.80G_{A,0}(\psi,\beta) + 0.05ST_{A,0}(F_y) + 0.15S_{A,0}(soil\ type) \\ A_{\mathrm{LDA}} = 0.80G_{A,\mathrm{LDA}}(\psi,\beta) + 0.05ST_{A,\mathrm{LDA}}(F_y) + 0.15S_{A,\mathrm{LDA}}(soil\ type) \\ A_{100} = 0.80G_{A,100}(\psi,\beta) + 0.05 \times ST_{A,100}(F_y) + 0.15S_{A,100}(soil\ type) \end{cases} \tag{22}$$

$$\begin{cases} B_0 = 0.80G_{B,0}(\psi,\beta) + 0.05ST_{B,0}(F_y) + 0.15S_{B,0}(soil\ type) \\ B_{\mathrm{LDA}} = 0.80 \times G_{B,\mathrm{LDA}}(\psi,\beta) + 0.05ST_{B,\mathrm{LDA}}(F_y) + 0.15S_{B,\mathrm{LDA}}(soil\ type) \\ B_{100} = 0.80G_{B,100}(\psi,\beta) + 0.05ST_{B,100}(F_y) + 0.15S_{B,100}(soil\ type) \end{cases} \tag{23}$$

This weighting indicates the governing importance of fault crossing geometry vis-à-vis the steel grade and the soil type. Although past literature has dealt with parts of this problem mostly, rather than considering all factors together, similar conclusions can be found in [42].

4.8 Evaluation and validation of the simplified expressions

To validate the proposed expressions outside the training data set, a distinct testing set is employed. It comprises four cases with widely dispersed arbitrary combinations of parameters (ψ,β), f_y, and soil type. It should be noted that regression is at its most accurate for the training set for which it has been optimized. The parameters were selected to test samples at the edges of the parameters' space, especially regarding steel grade and soil property effects, where only a central design was employed. The cases under examination and the resulting error metrics are presented in Table 14, where the important error metric for each is highlighted with bold. The following observations are derived from Table 14:

- The precision for the 0% local buckling limit is very high and close to 1.00. Lower values are observed for a marginal fault crossing geometry, namely for ψ = 30^{o} for ALA operable (precision = 0.79) and EN 1998-4 (precision = 0.73) limits.
- The precision for the 100% local buckling limit is generally over 0.90.
- The balanced accuracy for the LDA line is in general over 0.80, indicating that the overall performance of the statistical model is over 80%.
- Recall values are observed to be quite low especially for the 0% local buckling limit. This is indicative of the impossibility of clearly separating the predominant failure modes in the intermediate area.

The error metrics are deemed to be acceptable and sufficient for preliminary design purposes, considering the complexity and the multi-parametric nature of the problem.

Table 14: Cases under examination and corresponding error metrics for the validation of the methodology. Precision is the appropriate error metric for the 0% and 100% local buckling limits and is highlighted with bold because these limits are created for maximum precision. Balanced accuracy (highlighted with bold) is examined for the LDA in order to evaluate the overall performance of the statistic model.

	ALA operable limits			**0% local buckling**			**LDA**			**100% local buckling**		
Case No.	fault crossing geometry	steel grade	sandy soil	**precision**	recall	balanced accuracy	precision	recall	**balanced accuracy**	**precision**	recall	balanced accuracy
1	$\psi = 30^{o}$, $\beta = 60^{o}$	X56	loose	**0.79**	0.17	0.58	0.97	0.97	**0.84**	**0.99**	0.91	0.94
2	$\psi = 40^{o}$, $\beta = 80^{o}$	X80	dense	**0.92**	0.29	0.64	0.99	0.94	**0.92**	**1.00**	0.83	0.91
3	$\psi = 80^{o}$, $\beta = 60^{o}$	X70	loose	**1.00**	0.36	0.68	0.88	0.94	**0.84**	**0.97**	0.38	0.68
4	$\psi = 50^{o}$, $\beta = 70^{o}$	X100	medium	**1.00**	0.21	0.61	0.85	0.99	**0.83**	**0.91**	0.94	0.89
	ALA pressure integrity limits			**0% local buckling**			**LDA**			**100% local buckling**		
Case No.	fault crossing geometry	steel grade	sandy soil	**precision**	recall	balanced accuracy	precision	recall	**balanced accuracy**	**precision**	recall	balanced accuracy
1	$\psi = 30^{o}$, $\beta = 60^{o}$	X56	loose	**1.00**	0.22	0.61	0.93	0.92	**0.92**	**1.00**	0.67	0.83
2	$\psi = 40^{o}$, $\beta = 80^{o}$	X80	dense	**0.99**	0.71	0.85	0.98	0.81	**0.89**	**1.00**	0.38	0.69
3	$\psi = 80^{o}$, $\beta = 60^{o}$	X70	loose	**0.91**	0.26	0.60	0.74	0.84	**0.86**	**0.99**	0.59	0.79
4	$\psi = 50^{o}$, $\beta = 70^{o}$	X100	medium	**1.00**	0.64	0.82	0.81	0.98	**0.93**	**1.00**	0.51	0.75
	EN 1998-4 limits			**0% local buckling**			**LDA**			**100% local buckling**		
Case No.	fault crossing geometry	steel grade	sandy soil	**precision**	recall	balanced accuracy	precision	recall	**balanced accuracy**	**precision**	recall	balanced accuracy
1	$\psi = 30^{o}$, $\beta = 60^{o}$	X56	loose	**0.73**	0.22	0.61	0.98	0.98	**0.85**	**1.00**	0.90	0.95
2	$\psi = 40^{o}$, $\beta = 80^{o}$	X80	dense	**0.84**	0.37	0.68	0.99	0.94	**0.92**	**1.00**	0.81	0.91
3	$\psi = 80^{o}$, $\beta = 60^{o}$	X70	loose	**1.00**	0.43	0.72	0.95	0.96	**0.90**	**0.94**	0.79	0.83
4	$\psi = 50^{o}$, $\beta = 70^{o}$	X100	medium	**1.00**	0.22	0.61	0.83	1.00	**0.79**	**0.94**	0.92	0.90

4.9 Design application

The developed simplified expressions can be directly applied for design purposes. The required input data are (1) pipeline D/t ratio defined by the pipe process design, (2) fault dip angle ψ obtained from geological and geotechnical survey, (3) pipe – fault crossing angle β defined by the route selection procedure, and (4) burial depth H defined by pertinent codes (e.g. EN 1594 [58] and ISO 13686 [59]). Therefore, given the input data, the 0% local buckling and the 100% local buckling limits are defined. Then, given the D/t ratio and the burial depth H/D, the area that the pipe under consideration is located can be defined. In case the pipe is located in the only-local-buckling "area" (on the right-hand side of the 100% local buckling limit), then appropriate countermeasures against local buckling should be applied. In case the pipe is located in the no-local-buckling area (on the left-hand side of the 0% local buckling limit), then protection measures against upheaval buckling or tensile rupture should be considered. An overview of seismic countermeasures for pipes under faulting can be found in [60]-[61]. Finally, in case the pipe is located in the intermediate area, then a more thorough investigation by means of advanced analysis is needed. The process to apply the proposed methodology is summarized in Table 15.

Table 15: Steps of the proposed methodology for predicting the predominant failure mode of a pipe under reverse faulting

Step	Action
1	Pipe design parameters: diameter D, wall thickness t, burial depth H, steel grade f_y, fault dip angle ψ, pipe – fault crossing angle β and soil type
2	Calculate the dimensionless values of burial depth H/D, $\log(D/t)$ ratio, $F_y = f_y/448.50$, and categorize soil as per Table 4
3	Estimate the effect of fault crossing geometry $G(\psi,\beta)$ for the three limits using Eq. (16) and Table 5 through Table 7 depending on the adopted strain limits
4	Estimate the effect of steel grade $ST(F_y)$ for the three limits using Eq. (17) and Table 8 through Table 10 depending on the adopted strain limits
5	Estimate the effect of soil type S for the three limits using Table 11 through Table 13 and depending on the adopted strain limits
6	Calculate coefficients A and B via Eqs. (22) and (23), respectively, for 0% local buckling, LDA, and 100% local buckling limits
7	Predict the predominant failure mode using the following algorithm: Estimate Det_0 for the 0% local buckling limit after Eq. (11) Det_{LDA} for LDA after Eq. (12) Det_{100} for the 100% local buckling limit after Eq. (13) if $Det_{100} > 0$ then the predominant failure mode is local buckling else if $Det_0 < 0$ then the predominant failure mode is upheaval buckling or tensile fracture or one of these two, depending on the adopted code-based strain limits else if $Det_{LDA} > 0$ then local buckling is more likely to be the predominant failure mode else upheaval buckling or tensile fracture is more likely to be

8 If the predominant failure mode is well-defined then take necessary seismic countermeasures or re-design the pipe
else perform a more thorough analysis

5. Summary and conclusions

The main parameters affecting the mechanical behavior of buried pipelines subjected to reverse fault rupture are the pipe – fault crossing geometry, the diameter to thickness ratio (D/t) that defines the pipe local slenderness, the burial depth, the pipe steel grade, and the soil type. An extensive numerical parametric study has been carried out for a wide range of realistic design parameters. The first comprehensive attempt is offered to quantify the qualitative criterion of Yun and Kyriakides [4], which states that shallowly buried pipes with low D/t ratio tend to buckle globally, while deeply buried pipes with high D/t ratio tend to buckle locally. Numerical results have been statistically processed through a multi-stage fitting process, using full functional experiment and central composite experiment designs. Linear discriminant analysis has been implemented in the "D/t ratio – burial depth" space to discriminate the failure mode areas and build the statistical model. Three areas have been defined: (1) only-local-buckling area, where the pipe is expected to fail due to local buckling, (2) intermediate area, where failure modes cannot be separated in a reliable manner, and (3) no-local-buckling area, where the pipe is expected to fail due to upheaval buckling or tensile fracture. The methodology has been applied for the operable and the pressure integrity strain limits of the American Lifelines Alliance (ALA) and the strain limits of EN 1998-4.

The statistical processing of results has revealed that fault crossing geometry controls the pipe response, hence also the failure mode, to a greater extent, as it determines the level of bending and compression that the pipe exhibits. Then, soil properties have a small effect and steel grade has a minimal effect. The increase of sand density leads to the expansion of the only-local-buckling area in the "D/t ratio – burial depth" space due to the increase of soil resistance to the pipe movement in the trench, a fact that confirms the requirement for trench backfilling with loose soil material to avoid local failures caused by excessive compression. It was also found that the steel grade upgrade will cause some shrinking of the only-local-buckling area in the "D/t ratio – burial depth" space.

The derived expressions can be applied for the preliminary design of a buried pipe under reverse fault rupture. The pipe designer is thus able to pre-determine the predominant failure mode for the design case and standards at hand and consequently redirect the design procedure and/or consider appropriate seismic countermeasures.

Acknowledgments

The first two authors acknowledge the financial support provided by the European Union's Horizon 2020 research and innovation programme "INFRASTRESS-Improving resilience of sensitive industrial plants & infrastructures exposed to cyber-physical threats, by means of an open testbed stress-testing system" under grant agreement No. 833088.

References

[1] O'Rourke MJ, Liu X. Seismic design of buried and offshore pipelines. Monograph No. 4". Multidisciplinary Center for Earthquake Engineering Research, Buffalo, USA; 2012. http://www.eng.buffalo.edu/mceer-reports/12/12-MN04.pdf

[2] Psyrras N, Kwon O, Gerasimidis S, Sextos A. Can a buried gas pipeline experience local buckling during earthquake ground shaking? Soil Dyn Earthq Eng 2019;116:511-529. https://doi.org/10.1016/j.soildyn.2018.10.027

[3] Psyrras NK, Sextos AG. Safety of buried steel natural gas pipelines under earthquake-induced ground shaking: A review. Soil Dyn Earthq Eng 2018;106:254-277. https://doi.org/10.1016/j.soildyn.2017.12.020

[4] Yun HD, Kyriakides S. On the beam and shell modes of buckling of buried pipelines. Soil Dyn Earthq Eng 1990;9(4):179-193. https://doi.org/10.1016/S0267-7261(05)80009-0

[5] European Committee for Standardization. CEN EN 1998-4, Eurocode 8, Part 4: Silos, tanks and pipelines. Brussels, Belgium; 2006.

[6] ALA American Lifelines Alliance. Guideline for the design of buried steel pipe – July 2001 (with addenda through February 2005). American Society of Civil Engineers, New York, USA; 2005. https://www.americanlifelinesalliance.com/pdf/Update061305.pdf

[7] Canadian Standards Association. CSA-Z662 Oil and gas pipeline systems, Etobicoke, Canada; 2007.

[8] Karamitros DK, Bouckovalas GD, Kouretzis GD, Gkesouli V. An analytical method for strength verification of buried steel pipelines at normal fault crossings. Soil Dyn Earthq Eng 2011;31:1452-1464. https://doi.org/10.1016/j.soildyn.2011.05.012

[9] Trifonov OV, Cherniy VP. A semi-analytical approach to a nonlinear stress-strain analysis of buried steel pipelines crossing active faults. Soil Dyn Earthq Eng 2010;30:1298-1308. https://doi.org/10.1016/j.soildyn.2010.06.002

[10] Trifonov OV, Cherniy VP. Elastoplastic stress-strain analysis of buried steel pipelines subjected to fault displacement with account for service loads. Soil Dyn Earthq Eng 2012;33(1):54-62. https://doi.org/10.1016/j.soildyn.2010.06.002

[11] Zhang L, Zhao X, Yan X, Yan X. Elastoplastic analysis of mechanical response of buried pipelines under strike-slip faults. Int J Geomech 2016;04016109. https://doi.org/10.1061/(ASCE)GM.1943-5622.0000790

[12] Sarvanis GC, Karamanos SA. Analytical model for the strain analysis of continuous buried pipelines in geohazard areas. Eng Struct 2017;152:57-69. https://doi.org/10.1016/j.engstruct.2017.08.060

[13] Ogawa Y, Yanou Y, Kawakami M, Kurakake T. Numerical study for rupture behavior of buried gas pipeline subjected to seismic fault displacement. In Proceedings of the 13th World Conference on Earthquake Engineering. Vancouver, Canada, 2014.

[14] Joshi S, Prashant A, Deb A, Jain SK. Analysis of buried pipelines subjected to reverse fault motion. Soil Dyn Earthq Eng 2011;31(7):930-940. https://doi.org/10.1016/j.soildyn.2011.02.003

[15] Chaudhary V, Kumar PVD, Kumar RP. Finite element analysis of buried continuous pipeline subjected to fault motion. I J Struct Eng 2013;4(4):314-331. https://doi.org/10.1504/IJSTRUCTE.2013.056981

[16] Uckan E, Akbas B, Shen J, Rou W, Paolacci F, O'Rourke MJ. A simplified analysis model for determining the seismic response of buried steel pipes at strike-slip fault crossings. Soil Dyn Earthq Eng 2015;75:55-65. https://doi.org/10.1016/j.soildyn.2015.03.001

[17] Liu X, Zhang H, Han Y, Xia M, Zheng W. A semi-empirical model for peak strain prediction of buried X80 steel pipelines under compression and bending at strike-slip fault crossings. J Nat Gas Sci Eng 2016;32:465-475. https://doi.org/10.1016/j.soildyn.2015.03.001

[18] Vazouras P, Dakoulas P, Karamanos SA. Pip-soil interaction and pipeline performance under strike-slip fault movements. Soil Dyn Earthq Eng 2015;72:48-65. https://doi.org/10.1016/j.soildyn.2015.01.014

[19] Trifonov OV. Numerical stress-strain analysis of buried steel pipelines crossing active strike-slip faults with an emphasis on fault modeling aspects. J Pipeline Syst Eng Pract 2015;6(1):04014008. https://doi.org/10.1061/(ASCE)PS.1949-1204.0000177

[20] Rahman MA, Taniyama H. Analysis of a buried pipeline subjected to fault displacement: A DEM and FEM study. Soil Dyn Earthq Eng 2015;71:49-62. https://doi.org/10.1016/j.soildyn.2015.01.011

[21] Zhang J, Liang Z, Han CJ. Buckling behavior analysis of buried gas pipeline under strike-slip fault displacement. J Nat Gas Sc Eng 2014;21:901-928. https://doi.org/10.1016/j.jngse.2014.10.028

[22] Banushi G, Squelia N, Thiele K. Innovative analysis of a buried operating pipeline subjected to strike-slip fault movement. Soil Dyn Earthq Eng 2018;107:234-249. https://doi.org/10.1016/j.soildyn.2018.01.015

[23] Wijewickreme D, Karimian H, Honegger D. Response of buried steel pipelines subjected to relative axial soil movement. Can Geotech J 2009;46(7):735-752. https://doi.org/10.1139/T09-019

[24] Abdoun TH, Ha D, O'Rourke MJ, Symans MD, O'Rourke TD, Palmer MC, and Stewart HE. Factors influencing the behavior of buried pipelines subjected to earthquake faulting. Soil Dyn Earthq Eng 2009;29(3):415-427. https://doi.org/10.1016/j.soildyn.2008.04.006

[25] Ha D, Abdoun TH, O'Rourke MJ, Symans MD, O'Rourke TD, Palmer MC, Stewart HE. Earthquake faulting effects on buried pipelines – case history and centrifuge study. J Earthq Eng 2010;14(5):646-669. https://doi.org/10.1080/13632460903527955

[26] Moradi M, Rojhani M, Galandarzadeh A, Takada S. Centrifuge modeling of buried continuous pipelines subjected to normal faulting. Earthq Eng Eng Vib 2013;12(1):155-164. https://doi.org/10.1007/s11803-013-0159-z

[27] Sarvanis GC, Karamanos SA, Vazouras P, Mecozzi E, Lucci A, Dakoulas P. Permanent earthquake-induced actions in buried pipelines: Numerical modeling and experimental verification. Earth Eng Struct Dyn 2018;47(4):966-987. https://doi.org/10.1002/eqe.3001

[28] Newmark NM, Hall WJ. Pipeline design to resist large fault displacement. In: Proceedings of the US National Conference on Earthquake Engineering, 1975 Jun 18-20, Ann Arbor, Michigan, USA.

[29] Rojhani M, Moradi M, Galandarzadeh A, Takada S. Centrifuge modeling of buried continuous pipelines subjected to reverse faulting. Can Geotech J 2012;49:659-670. https://doi.org/10.1139/t2012-022

[30] Rofooei FR, Jalali HH, Attari NKA, Kenarangi H, Samadian M. Parametric study of buried steel and HDPE gas pipelines due to oblique-reverse faulting. Can J Civ Eng 2015;42(3):178-89. https://doi.org/10.1139/cjce-2014-0047

[31] Zhang J, Liang Z, Han CJ, Zhang H. Numerical simulation of buckling behavior of the buried steel pipeline under reverse fault displacement. Mech Sc 2015;6:203-210. https://doi.org/10.5194/ms-6-203-2015

[32] Jalali HH, Rofooei FR, Attari NKA, Samadian M. Experimental and finite element study of the reverse faulting effects on buried continuous steel gas pipelines. Soil Dyn Earthq Eng 2016;86:1-14. https://dx.doi.org/10.1016/j.soildyn.206.04.006

[33] Liu X, Zhang H, Li M, Xia M, Zheng W, Wu K, Han Y. Effects of steel properties on the local buckling response of high strength pipelines subjected to reverse faulting. J Nat Gas Sci Eng 2016;33:378-387. https://doi.org/10.1016/j.jngse.2016.05.036

[34] Liu X, Zhang H, Wu K, Xia M, Chen Y, Li M. Buckling failure mode of buried X80 steel gas pipeline under reverse fault displacement. Eng Fail Anal 2017;77:50-64. https://doi.org/10.1016/j.engfailanal.2017.02.019

[35] Xu L, Lin M. Analysis of buried pipelines subjected to reverse fault motion using the vector form intrinsic element method. Soil Dyn Earthq Eng 2017;93:61-83. https://doi.org/10.1016/j.soildyn.2016.12.004

[36] Wijewickreme D, Monroy M, Honegger DG, Nyman DJ. Soil restraints on buried pipelines subjected to reverse fault displacement. Can Geotech J 2017;54(10):1472-1481. https://doi.org/10.1139/cgj-2016-0564

[37] Jalali HH, Rofooei FR, Attari NKA. Performance of buried gas distribution pipelines subjected to reverse fault motion. J Earthq Eng 2018;22(6):1068-1091. https://doi.org/10.1080/13632469.2016.1269694

[38] Rofooei FR, Attari NKA, Jalali HH. New method of modeling the behavior of buried steel distribution pipes subjected to reverse faulting. J Pipeline Syst Eng Pract 2018;9(1):04017029. https://doi.org/10.1061/(ASCE)PS.1949-1204.0000296

[39] PRCI (Pipeline Research Council International). Guidelines for constructing natural gas and liquid hydrocarbon pipelines through areas prone to landslide and subsidence hazards. Final Rep to PRCI on Project ENV-1, Chantilly, VA, USA, 2009.

[40] Demirci HE, Bhattacharya S, Karamitros D, Alexander N. Experimental and numerical modeling of buried pipelines crossing reverse faults. Soil Dyn Earthq Eng 2018;114:198-214. https://doi.org/10.1016/j.soildyn.2018.06.013

[41] Cheng X, Ma C, Huang R, Huang S, Yang W. Failure mode analysis of X80 buried steel pipeline under oblique-reverse fault. Soil Dyn Earthq Eng 2019;125:105723. https://doi.org/10.1016/j.soildyn.2019.105723

[42] Tsatsis A, Loli M, Gazetas G. Pipeline in dense sand subjected to tectonic deformation from normal and reverse faulting. Soil Dyn Earthq Eng 2019;127:105780. https://doi.org/10.1016/j.soildyn.2019.105780

[43] Zhang J, Chen Y, Zhang H. Local buckling evolution mechanism of a buried steel pipe under fault movements. Energy Sci Eng 2019;00:1-14. https://doi.org/10.1002/ese3.524

[44] Shi R, Wang L, Guo Z, Yuan F. Upheaval buckling of a pipeline with prop imperfection on a plastic seabed. Thin Wall Struct 2013;65:1-6. https://doi.org/10.1016/j.tws.2012.12.008

[45] Taylor N, Gan AB. Submarine pipeline buckling – imperfection studies. Thin Wall Struct 1986;4:295-323. https://doi.org/10.1016/0263-8231(86)90035-2

[46] Wang L, Shi R, Yuan F, Guo Z, Yu L, Global buckling of pipeline in the vertical plane with soft seabed. Appl Ocean Res 2011;33:130-136. https://doi.org/10.1016/j.apor.2011.01.002

[47] ADINA R & D Inc. ADINA 9.3.3 Release Notes, Watertown, USA; 2017.

[48] Melissianos VE, Gantes CJ. Numerical modeling aspects of buried pipeline – fault crossing. In: Papadrakakis M, Plevris V, Lagaros ND (EDS). Computational Methods in Earthquake Engineering, Computational Methods in Applied Sciences, VOL. 44. Berlin: Springer Verlag; 2017, p 1-26. https://doi.org/10.1007/978-3-319-47798-5_1

[49] Melissianos VE, Korakitis GP, Gantes CJ, Bouckovalas GD. Numerical evaluation of the effectiveness of flexible joints in buried pipelines subjected to strike-slip fault rupture. Soil Dyn Earthq Eng 2016;90:395-410. https://doi.org/10.1016/j.soildyn.2016.09.012

[50] Melissianos VE, Lignos XA, Bachas KK, Gantes CJ. Experimental investigation of pipes with flexible joints under fault rupture. J Constr Steel Res 2017;128:633-648. https://doi.org/10.1016/j.jcsr.2016.09.026

[51] Bathe KJ, Almeida CA. A simple and effective pipe elbow element – linear analysis. J Appl Mech, Transactions of the ASME 1980;47(1):93-100. https://doi.org/10.1115/1.3153645

[52] Bathe KJ, Almeida CA, Ho LW. A simple and effective pipe elbow element – some nonlinear capabilities. Comp & Structures 1983;17(5/6):659-669. https://doi.org/10.1016/0045-7949(83)90079-2

[53] American Petroleum Institute. API Specification 5L Specification for Line Pipe, 46th edition, Washington, DC, USA; 2018.

[54] McLachlan GJ. Discriminant analysis and statistical pattern recognition. Wiley, New Jersey, USA; 2004. https://doi.org/10.1002/0471725293

[55] Box GE, Hunter WG, Hunter JS. Statistics for experimenters: design, innovation, and discovery, 2nd edition. Wiley, Hoboken, New Jersey, United States; 2005.

[56] Liu X, Zhang H, Han Y, Xia M, Zheng W. A semi-empirical model for peak strain prediction of buried X80 steel pipelines under compression and bending at strike-slip fault crossing. J Nat Gas Sci Eng 2016;32:465-475. https://doi.org/10.1016/j.jngse.2016.04.054

[57] Olson DL, Delen D. Advanced data mining techniques, 1st edition. Springer, Berlin, Germany; 2008. https://doi.org/10.1007/978-3-540-76917-0

[58] British Standards Institution. BS EN 1594:2013 Gas infrastructure. Pipelines for maximum operating pressure over 16 bar. Functional requirements. London, UK; 2013.

[59] Internation Organization for Standardization. ISO 13686:2013 Natural gas - Quality designation, Geneva, Switzerland; 2013.

[60] Gantes CJ, Melissianos VE. Evaluation of seismic protection methods for buried fuel pipelines subjected to fault rupture. Front Built Environ 2016;2:34. https://doi.org/10.3389/fbuil.2016.00034

[61] Melissianos VE, Gantes CJ. Protection measures for buried steel pipelines subjected to fault rupture. In: Proceedings of the 2nd International Conference on Natural Hazards & Infrastructure, 2019 Jun 23-26, Chania, Greece.